

Effects of carbon concentration and filament number on advanced internal-Mg-infiltration-processed MgB₂ Strands

G Z Li¹, M D Sumption¹, J B Zwyer¹, M A Susner¹, M A Rindfleisch², C J Thong², M J Tomsic² and E W Collings¹

¹ Center for Superconducting and Magnetic Materials, Department of Materials Science and Engineering, the Ohio State University, Columbus, OH 43210, U.S.A.

² Hyper Tech Research Incorporated, 539 Industrial Mile Road, Columbus, OH 43228, U.S.A.

Abstract

An advanced internal Mg infiltration method (AIMI) in this paper has been shown to be effective in producing superconducting wires containing dense MgB₂ layers with high critical current densities. In this study, the in-field critical current densities of a series of AIMI-fabricated MgB₂ strands were investigated in terms of C doping levels, heat treatment (HT) time and filament numbers. The highest layer J_c for our monofilamentary AIMI strands is 1.5×10^5 A/cm² at 10 T, 4.2 K, when the C concentration was 3 mol% and the strand was heat-treated at 675 °C for 4 hours. Transport critical currents were also measured at 4.2 K on short samples and one-meter segments of eighteen-filament C-doped AIMI strands. The layer J_c s reached 4.3×10^5 A/cm² at 5 T and 7.1×10^4 A/cm² at 10 T, twice as high as those of the best PIT strands. The analysis of these results indicates that the AIMI strands, possessing both high layer J_c s and engineering J_e s after further optimization, have strong potential for commercial applications.

PACS: 74.70.Ad; 74.25.Sv; 74.25.Qt; 74.62.Dh

Keywords: MgB₂, advanced internal Mg infiltration, AIMI, second generation, 2G, 2G-IMD, internal-Mg-diffusion, IMD, reactive liquid-Mg infiltration, Mg-RLI, layer critical current density, J_c , non-barrier critical current density, engineering critical current density, J_e

1. Introduction

Extensive efforts have been made to improve the transport properties of superconductors based on MgB_2 since the discovery of its superconducting properties in 2001 [1]. Typical MgB_2 powder-in-tube (PIT) wires, consisting of an MgB_2 core surrounded by a chemical barrier and a hard outer sheath, can be made by either the *ex situ* or the *in situ* routes [2]. Through the *ex situ* technique, it is possible to develop homogeneous MgB_2 wires with high powder packing densities over long lengths [3]. Since the powder fill consists of pre-reacted MgB_2 , the wires can be used either as-formed or after a sintering heat treatment (HT) at temperatures of around 800-900 °C [4, 5]. The *in situ* wires need to be heat-treated in order to react the mixed Mg and B powders. Typical HT temperatures are 650-800 °C [6, 7] although lower temperatures, even below the melting point of Mg, have been used [8]. High porosity and weak connectivity are critical issues associated with conventional *in situ* PIT MgB_2 wires [9], even though they have some of the highest J_c values present in the literatures [10, 11].

An interesting variant of the *in situ* PIT route is the “internal Mg diffusion” (IMD) process or the “reactive liquid-Mg infiltration” (Mg-RLI) process initiated by Giunchi *et al.* [12, 13]. The conductor is formed by Mg from the central rod diffusing into the surrounding B precursors in certain conditions and then reacting into a MgB_2 hollow cylinder. Whereas the PIT process produces a porous MgB_2 core, the IMD process provides a dense MgB_2 layer with excellent longitudinal and transverse connectivities [14-16]. To calculate the critical current densities of these IMD wires, it is important to take care with the definition of the areas to which the critical current, I_c , is normalized. Three areas are commonly used depending on different purposes [17]: (a) the layer

critical current density, layer J_c , is defined by using the cross-sectional area of MgB_2 in the composite. All the other components, including the central hole in IMD wires, are ignored; (b) the non-barrier critical current density, non-barrier J_c , takes into consideration the cross-sectional area of everything within the chemical barrier. It is best used for direct quality comparison between different types of MgB_2 wires; (c) the engineering critical current density, J_e , adopts the cross-sectional area of the entire strand. This is an important parameter for engineering designs.

Numerous attempts have been made to develop high performing IMD wires, including doping [18], adding extra Mg into B layers to assist the MgB_2 layer growth [19], optimizing HT conditions [20], and adjusting filament numbers and wire geometries [21, 22]. Adding different kinds of chemicals into wires, such as SiC [21] and liquid aromatic hydrocarbon [23], were proved to achieve layer J_c s and engineering J_e s, which are much higher than undoped IMD wires. For example, Kumakura *et al.* [21] fabricated a series of 10 mol% SiC doped MgB_2 wires using the IMD process. A high layer J_c of 1.1×10^5 A/cm² was attained at 4.2 K and 10 T for one of their monofilamentary wires HTed at 600 °C. By using C doped nano-sized amorphous B powders, our group also made IMD wires with a good layer J_c of 1.0×10^5 A/cm² obtained at 4.2 K and 10 T [16]. Also, Togano *et al.* [20] prepared a series of multifilamentary IMD wires. They considered the nineteen-filamentary IMD wires as optimal candidates for high performing strands, because the fine filaments in the nineteen-filamentary IMD wires enabled a thinner MgB_2 layer and hence were more suitable to gain full MgB_2 phase transformation. A good layer J_c of 9.9×10^4 A/cm² was obtained for their nineteen-filamentary IMD wire at 4.2 K and 10 T. However, given the low “ MgB_2 fill factor”, (i.e. the effective MgB_2 cross sectional area fraction in the whole strand), this wire only achieved the engineering J_e of less than

3×10^3 A/cm² at 4.2 K and 10 T, even though the B in it has been nearly fully transformed into MgB₂.

Nevertheless, because the maximum MgB₂ layer thickness was always limited to 20-30 μ m [20], the J_{eS} of all of these IMD wires were actually lower than state of the art PIT wires. To overcome the limitations of MgB₂ layer thickness in previous IMD wires, our group studied the MgB₂ layer growth mechanism associated with the Mg diffusion route. In our recent report [24], our efforts in choosing optimized B powder types, various wires diameters, HT conditions and wire constructions finally led to high performing wires with maximum layer J_c of 1.1×10^5 A/cm² and maximum engineering J_e of 1.7×10^4 A/cm² at 4.2 K and 10 T. The J_{eS} for those samples were now much higher than those of best of class PIT strands. To indicate the substantial advances in the capabilities of these “second generation” MgB₂ strands, and to point to the large quantitative difference in the practical properties between these conductors and previous wires, we describe these “ J_e -optimized” strands as “advanced internal Mg infiltration” (AIMI) wires.

Although it was widely reported that dopants, especially C and carbides, were beneficial in enhancing the layer J_c and engineering J_e , the effect of the C doping level on these properties has not been systematically investigated in either early IMD-synthesized wires or our new AIMI wires. So it is necessary to figure out the optimal C concentration for the AIMI wires. Moreover, considering the excellent layer J_c and engineering J_e properties of monocoil AIMI strands, it is also essential to develop multifilamentary AIMI wires for application. In addition, most reports about the diffusion or infiltration-processed wires to date have focused on short wires (e.g. \ll 1 m total length); only a few measurements have been made on long strands [22] although a one-meter-long undoped Mg-RLI monofilament wire fabricated by Giunchi *et al.* had a engineering J_e of over 1.0

$\times 10^4$ A/cm² at 4.2 K and 5 T [25]. Though the AIMI wires have higher layer J_c s than their PIT counterparts, many other characteristics such as engineering J_e , MgB₂ fill factor and thermal stability need to be optimized in long wires before this manufacturing process is applied commercially.

For this study a group of 3 mol% and 4 mol% C doped monofilamentary “advanced internal Mg infiltration-processed” (AIMI) strands have been fabricated and compared with the previously reported 2 mol% C monocoil strand. The critical transport currents were measured and the results were reported in terms of layer J_c s and non-barrier J_c s after the appropriate cross sectional areas were measured by scanning electron microscopy (SEM). The effects of C doping level on the layer J_c s and microstructures of the monofilamentary wires have been studied. Multifilamentary strands of eighteen sub-elements were also prepared using the same C-doping concentrations. Their respective values of layer J_c , non-barrier J_c and engineering J_e were then compared with a set of conventional multifilamentary PIT strands at 4.2 K. In particular, the 2 mol% C doped eighteen-filamentary AIMI wires were made into one-meter-long strands for the purpose of large scale characterization of the superconducting properties of the AIMI strands.

2. Experimental

2.1 Sample preparation

In this paper, three groups of MgB₂ strands, including (i) monofilamentary AIMI strands, (ii) multifilamentary AIMI strands and (iii) typical multifilamentary PIT strands, were manufactured by Hyper Tech Research Inc. (HTR). All strands used the C-doped B

powder produced by the plasma assisted reaction between BCl_3 , H_2 and suitable amount of CH_4 (Specialty Materials Inc., SMI) [26]. This powder was mostly amorphous, 10-100 nm in size, with C doping levels ranging from 2 mol% to 4 mol%.

The wire fabrication procedure is described as follow: (i) The strand geometry of the monofilamentary AIMI strands were based on our previous studies of 2 mol% C doped “2G-IMD” strands [24] and 2-4 mol% C doped PIT strands [27]. The starting billet was a Mg rod positioned along the axis of a B-filled double tube of Nb and Monel; the B is doped with either 3 mol% or 4 mol% C. Then the billet was drawn to 0.55 mm outer diameter (OD). (ii) To fabricate multifilamentary AIMI strands, the initial billet, of the same geometry as that of monofilamentary AIMI strands, was drawn to an intermediate-sized monofilament. Then the eighteen of these monofilaments and one central Cu-Ni alloy filament were restacked into a Monel tube, and further drawn to an OD of 0.83 mm. (iii) To compare with multifilamentary AIMI strands in terms of critical current densities, a group of thirty-six-filamentary PIT strands with variable C doping levels were fabricated by HTR, using the “continuous tube filling-and-forming (CTFF)” approach [28]. As before the starting monofilamentary PIT strands were drawn to smaller diameter. Then thirty six as-drawn monofilaments together with a central Cu filament were restacked into a Monel tube and further drawn to 0.92 mm OD prior to HT.

After wire drawing, the three sets of strands were placed in a tube furnace respectively, ramped to soak temperature in about 80 min, kept at certain temperature for one, two or four hours and furnace cooled to room temperature. Since in this study we mainly considered the effect of HT time on MgB_2 wires, the HT temperature of 675 °C was chosen for all AIMI strands and most PIT strands. In fact, 675 °C is often regarded as the optimal temperature for CTFF-type PIT wires and little variation in J_c was found

with HT temperature at 650-700 °C for suitable times. Furthermore, all HT time was below 4 hours because longer sintering time would cause MgB₂ grain coarsening which were harmful for MgB₂ conductors. The strand specifications and HT conditions of the above mentioned three groups of strands are listed in table 1.

2.2 Characterization

Transport voltage-current measurements were performed on all samples at 4.2 K in pool boiling liquid He in transverse magnetic fields, B , of up to 13.5 T. Two types of samples were studied in this work: (1) “Short” straight samples 50 mm long, with a gauge length of about 5 mm. (2) “ITER-barrel” samples made with one-meter-long segments helically wound onto 32-mm-diameter Ti-Al-V alloy holders [28]. The gauge length was 500 mm. In both cases, the transport critical current was determined under an electric field criterion of 1 μ V/cm.

The microstructures of the MgB₂ wires, including the areas of the reacted MgB₂ layers, were characterized by scanning electron microscopy (SEM) and compositions quantified using energy dispersive X-ray spectroscopy (EDS). SEM observation was carried out using FEI (Philips) Sirion field-emission source SEM and Quanta 200 SEM equipped with the EDAX EDS system. Microstructures were also characterized using Olympus PME-3 optical microscope (OM) to obtain better contrast between MgB₂ and B layers.

3. Results

3.1 Monofilamentary AIMI strands

Figure 1 shows the layer J_c s of the 3 mol% and 4 mol% C doped monofilamentary MgB₂ strands at 4.2 K in magnetic field of 5-13.5 T. A previously reported 2 mol% C doped “2G-IMD” strand HTed at 675 °C for 1 hour [24] is also included in this plot for comparison. As the C doping level increases from 2 mol%, the layer J_c s of the AIMI strands are firstly enhanced at 3 mol% C and then suppressed when the C concentration is 4 mol%. The 3 mol% C doped sample A3 achieves the highest layer J_c of 1.5×10^5 A/cm² at 10 T. Also, it is noted that the layer J_c s of all samples, except A5, increase as the strands are heat treated longer. Take the 3 mol% C doped strands for example, after 1 hour HT, the layer J_c at 10 T is 1.3×10^5 A/cm² for A1. It increases to 1.4×10^5 A/cm² after 2 hours HT and finally attains 1.5×10^5 A/cm² after 4 hours HT.

Although moderately increasing C concentration from 2 mol% to 3 mol% is effective in improving the layer J_c , the transverse cross sectional view of the strands shows that the MgB₂ layer growth is suppressed for 3 mol% C doped strands and thus the MgB₂ layer thickness becomes relatively narrower than the 2 mol% C strands. Figure 2 shows the OM and back scattered SEM images of strand A3. They are taken from the same transverse cross section of the wire. Because of better contrast, the OM picture is helpful to discern the MgB₂ and B-rich layers. As indicated in figure 2(a), the orange (or purple) annulus is the MgB₂ layer and the outside dark area is the B-rich region. The MgB₂ layer looks dense but its layer thickness is limited – only 8-25 μm, which is less than a quarter of the maximum layer thickness of the previously reported 2 mol% C sample [24] under the same HT condition. The suppression of the MgB₂ layer growth caused by the carbide doping has also been reported by other groups [21], but the underlying mechanism is still

unclear. Consequently not only the area of MgB_2 and central Mg but also the area occupied by the non-superconducting B-rich region is taken into account as the total area to calculate the non-barrier J_c s of the wires. Therefore the non-barrier J_c s of these samples are reduced compared with the fully reacted AIMI strands.

Figure 3 shows the field dependence of the non-barrier J_c s for all of the monofilamentary strands. Sample A3 obtains the highest non-barrier J_c of 2.4×10^4 A/cm² at 10 T. This value is lower than that of the fully reacted 2 mol% C doped AIMI strand, but is still comparable to the non-barrier J_c s of most PIT wires [16]. Given the high layer J_c s of the 3 mol% C doped AIMI strands, there might be a great improvement in non-barrier J_c s once the full MgB_2 reaction could be realized.

3.2 Multifilamentary AIMI and PIT strands

Figure 4(a), the transverse cross-sectional SEM image of strand B1, represents the strand geometry of all multifilamentary AIMI samples. In the transverse direction, all subfilaments are about 100 μm in size and uniformly deformed. Mg and dispersed powders are found existing in the “prior-Mg” holes in the centers of filaments. Between the Nb barriers and the holes are the reacted MgB_2 layers with thickness of 0-30 μm . After increasing the contrast and brightness of figure 4(a) by 50% and thus the contrast difference within the reaction layers, it is found that only in some filaments has the B powder become fully transformed to MgB_2 . This is exemplified by the OM picture (Figure 4b), in which some filaments have grey B-rich areas outside the yellow MgB_2 circulars, indicating partially transformation. The structure of these multifilamentary strands is also examined longitudinally. Tubular MgB_2 layers are seen attached to the Nb

barriers in each filament. These MgB₂ filaments are uniform in diameter along the longitudinal direction. However, Nb barrier breakages can be seen at some locations. It is also noted that for every multifilamentary AIMI strand some residual Mg remains in the region of the break. EDS, employed to analyze the composition of the remaining Mg region for strand B3 and B5, detects the presence of Mg and Cu in the atomic ratio of about 4:5, implying that Cu has leaked into the filaments.

The areas of the MgB₂ layers are measured based on the transverse SEM images. Since both B and Mg are light atoms, the weak contrast in SEM figures between MgB₂ and other borides or B makes measurement difficult even when the contrast and brightness of the pictures are adjusted. So OM images, with better phase contrast, are used to assist distinguishing the MgB₂ region. Table 2 lists the MgB₂ areas as well as the MgB₂ fill factors of all multifilamentary AIMI samples obtained using this method. It is important to note that the MgB₂ fill factors of the present AIMI strands are only 9.2 to 14.6 %, significantly lower than those of PIT strands.

The field dependencies of the layer J_c s at 4.2 K for all the multifilamentary AIMI strands are shown in figure 5. Those of the two best performing PIT strands, P3 and P4, are also included for comparison. The best performing strand in magnetic field below 10 T is the 2 mol% C doped strand B1. At 5 T its layer J_c reaches 4.3×10^5 A/cm²; at 10 T it is 7.1×10^4 A/cm² which is twice as high as that achieved by the best PIT strand (i.e. the 3 mol% C-doped strand P3). The 4 mol% C doped strand B5 exhibits the highest layer J_c s at high fields above 10 T, although its low-field J_c s are lower than those of other strands. Its layer J_c attains 2.8×10^4 A/cm² at 13 T. Compared with B1 and B5, the 3 mol% C doped strand B3 shows good layer J_c s in all applied fields. But unlike its monofilamentary counterpart A1, a slightly heavier doping in multifilamentary AIMI

strands does not result in an appreciable layer J_c enhancement as compared with 2 mol% C doped AIMI wires. Secondly, it is noticeable that all the 2-hours-HT strands (i.e. B2, B4 and B6) show deteriorated layer J_c s as compared to their 1-hour-HT counterparts B1, B3 and B5 respectively. For example, after two hours HT, the layer J_c of what then becomes strand B2 decreases to 3.3×10^5 A/cm² at 5 T and 4.7×10^4 A/cm² at 10 T. However, the layer J_c s of B2 are still 30% higher than the best PIT results. Also this 1 m long ITER-barrel mounted AIMI strand shows comparable layer J_c s with other AIMI short samples, indicating the strand is uniform in the wire direction over long lengths, and it is capable of carrying a transport current of over 1000 A at 1 T, exhibiting excellent thermal stability. Figure 6 shows the non-barrier J_c vs. $\mu_0 H$ curves of the multifilamentary AIMI wires.

For the magnet builder the transport property of importance is the engineering J_e . Figure 7 presents J_e as a function of applied field strength. Since J_e is the critical current, I_c , divided by the transverse cross-sectional area of the whole wire, it also satisfies the relationship $J_e = \text{layer } J_c \times \text{MgB}_2 \text{ fill factor}$. The J_e of the best multifilamentary AIMI strand, B1, is 5.7×10^4 A/cm² at 5 T and 9.4×10^3 A/cm² at 10 T. Driven by their greater fill factors the best PIT results are here shown to be comparable to those of the best AIMI strands.

4. Discussion

The C or carbide doping concentration has been reported to have a great impact on the critical current densities of the conventional MgB₂ PIT wires [29, 30]. This effect still works for the monofilamentary AIMI strands. The monocoresh AIMI strands achieve

maximum layer J_{cs} when the C doping concentration is in the vicinity of 3 mol%. The layer J_c is suppressed when the C doping level deviates from this optimal value. This is in agreement with our group's previous results that the PIT strands behave best when the 3 mol% C is mixed into the wires [16, 27]. Proper carbon doping is proved to enhance the upper critical field B_{c2} , decrease the anisotropy ratio γ and provide extra flux pinning centers [27, 31, 32], all of which are helpful to obtain higher layer J_{cs} . Nevertheless, if too much C is doped, it might deteriorate the connectivity and thus reduce the transport layer J_{cs} [33]. As a consequence, relatively low layer J_{cs} are obtained for 4 mol% C samples when the C doping level is above 3 mol%. Compared with monofilamentary AIMI strands, the multifilamentary AIMI strands possess finer subfilaments and thus are more easily to suffer from degradations during the process of wire fabrication. The Nb barrier breakage observed in B1 and Cu leakage detected in samples B3 and B5 would cause a certain level of deterioration in layer J_{cs} , so the layer J_{cs} of all multifilamentary AIMI strands with any C doping level are lower than those of their monofilamentary counterparts. For the same reason, these extrinsic defects such as Cu contamination have so negative effects on multifilamentary wires that no obvious layer J_c improvement is observed even when the C doping level is optimal (i.e. 3 mol%).

The effect of HT time on the layer J_c is quite opposite for monofilamentary and multifilamentary AIMI strands. A longer HT time, such as 4 hours, is desired for monofilamentary AIMI strands, while a shorter period of HT time is more preferred in multifilamentary strands. The average B precursor layer thickness in multifilamentary strands is less than 20 μm , so the whole layer quickly transforms into MgB_2 within 1 hour during the HT. Extending HT time is not helpful for MgB_2 layer growth but could only cause grain coarsening, oxidation or Cu contamination, which are harmful for the strands

[34]. Contrarily, the average layer thickness of B precursor in monofilamentary AIMI strands is thicker than $50 \mu\text{m}$. So Mg is not able to diffuse deeply into the B layer within a short time. According to the MgB_2 layer growth mechanism in AIMI wires discussed in the early paper [24], a partially reacted MgB_2 layer is formed at the very beginning of HT, so moderate J_{cs} are obtained for A1. As HT continues, the MgB_2 layer becomes thicker, better transformed and well-connected. Consequently, A2 and A3 achieve improved J_{cs} and J_{es} .

The above difference also implies that multifilamentary AIMI MgB_2 wires are more advantageous to obtain high layer J_{cs} and engineering J_{es} than monocoil AIMI wires. They could be fully reacted within a short time, because the B precursor layers become narrower and thus the Mg diffusion distance is shortened. As the HT is completed faster, the grain coarsening can be prevented, and other detrimental effects like oxidation could be limited to a low level. Also, since the maximum MgB_2 layer thickness is always limited to a very small value (for example, $25 \mu\text{m}$ for 3 mol% C doped monofilamentary AIMI strands), it is desirable to reduce the thickness of the B precursor layer below the $25 \mu\text{m}$, which can be realized in multifilamentary strands.

The 10 T data of Figures 5 and 7 are combined in Figure 8. Given that layer $J_c \times FF = J_e$ (where FF represents the MgB_2 fill factor) plots of layer J_c vs. FF are rectangular hyperbolae corresponding to various selected values of J_e . For any given value of J_e there exists a reciprocal relationship between layer J_c and FF which leads in this case to a clustering of the AIMI data around high layer J_c and low FF and conversely for the PIT data. This occurs for the following reason: the MgB_2 core of the PIT strands, which occupies some 25% of the strand cross section, being formed by the *in situ* reaction of Mg and B powders is porous. As a result of this, and the fact that the reacted MgB_2 exists

in the form of imperfectly connected stringers [35], the longitudinal critical current density (the layer J_c in the case of PIT) is relatively low as seen in the figure. In the AIMI strand the cylindrical MgB_2 layer is dense, well connected, and free of pores [22]. This leads to a high layer J_c . On the other hand the relative volume of the reacted layer (the AIMI strand's FF) tends to be small. It is possible, therefore for the AIMI data and the PIT data to cluster around a common J_e curve, but different segments of it. This tendency is seen for AIMI strands B5, B6, and B2 and PIT strands P1, P2, and P5. What Figure 8 tells us, however, is that having optimized the starting powders (Mg plus fine SMI B doped with 2-3 mol% C) and after improving strand processing to eliminate breakages and barrier leakages, a significant increase in J_e to much more than 10 kA/cm^2 at 4.2 K, 10 T, will accompany an increase in the FF of the AIMI strand.

5. Summary

The in-field critical current densities of a series of advanced internal Mg infiltration-processed MgB_2 strands have been investigated in terms of C doping level, HT time and filament number. The best monofilamentary AIMI strand A3, with 3 mol% C and under 4 hours HT at $675 \text{ }^\circ\text{C}$, achieves high layer J_c of $1.5 \times 10^5 \text{ A/cm}^2$ and non-barrier J_c of $2.4 \times 10^4 \text{ A/cm}^2$ at 10 T and 4.2 K. In multifilamentary AIMI strands, we have not retained the full layer J_c increase due to some defect structure. Even so, their layer J_c s, non-barrier J_c s and engineering J_e s are still better than, or at least comparable to, those of the best PIT strands. The one-meter-long version of the multifilamentary strands show that this kind of advanced MgB_2 strands is uniform and thermally stable, capable of being utilized in industry.

Acknowledgements

This work is funded by the Department of Energy, High Energy Physics division under Grant No. DE-FG02-95ER40900, a DOE SBIR, and a program from the Ohio Department of Development. The authors thank Dr. Yi Ding from Southeast University for his assistance in sample characterization and helpful discussions.

References

- [1] Nagamatsu J, Nakagawa N, Muranaka T, Zenitani Y and Akimitsu J 2001 Superconductivity at 39 K in magnesium diboride *Nature* **410** 63.
- [2] Glowacki B A, Majoros M, Vickers M, Evetts J E, Shi Y and McDougall I 2001 Superconductivity of powder-in-tube MgB₂ wires *Supercond. Sci. Technol.* **14** 193.
- [3] Braccini V, Nardelli D, Penco R and Grasso G 2007 Development of *ex situ* processed MgB₂ wires and their applications to magnets *Physica C* **456** 209.
- [4] Grasso G, Malagoli A, Ferdeghini C, Roncallo S, Braccini V, Siri A S and Cimberle M R 2001 Large transport critical currents in unsintered MgB₂ superconducting tapes *Appl. Phys. Lett.* **79** 230.
- [5] Tanaka H, Yamamoto A, Shimoyama J, Ogino H and Kishio K 2012 Strongly connected *ex situ* MgB₂ polycrystalline bulks fabricated by solid-state self-sintering *Supercond. Sci. Technol.* **25** 115022.
- [6] Kim J H, Oh S, Kumakura H, Matsumoto A, Heo Y, Song K, Kang Y, Maeda M, Rindfleisch M, Tomsic M, Choi S and Dou S X 2011 Tailored materials for high-performance MgB₂ wire *Adv. Mater.* **23** 4942.
- [7] Li G Z, Reddy K M, Zwayer J B, Kuldell M A, Susner M A, Yang Y, Sumption M D, Yue J J, Rindfleisch M A, Tomsic M J, Chong C J, and Collings E W 2013 Critical current density and current transfer length of multifilamentary MgB₂ strands of various design *IEEE Trans. Appl. Supercond.* **23** 6200204.
- [8] Pan X, Matsumoto A, Kumakura H, Zhao Y, Yan G and Feng Y 2012 Combined effect of upper critical field and flux pinning on enhancing critical current density of *in-situ* MgB₂/Fe tapes with various carbon sources simultaneously doped *Appl. Phys. Express* **5** 013102.
- [9] Collings E W, Sumption M D, Bhatia M, Susner M A and Bohnenstiehl S D 2008 Prospects for improving the intrinsic and extrinsic properties of magnesium diboride superconducting strands *Supercond. Sci. Technol.* **21** 103001.
- [10] Häbler W, Herrmann M, Rodig C, Schubert M, Nenkov K and Holzapfel B 2008 Further increase of the critical current density of MgB₂ tapes with nanocarbon-doped mechanically alloyed precursor *Supercond. Sci. Technol.* **21** 062001.
- [11] Wang D, Wang C, Zhang X, Gao Z, Yao C, Ma Y, Kanazawa M, Yamada Y, Oguro H, Awaji S and Watanabe K 2012 Enhancement of *J_c-B* properties for binary and carbon-doped MgB₂ tapes by hot pressing *Supercond. Sci. Technol.* **25** 065013.
- [12] Giunchi G, Ceresara S, Ripamonti G, Di Zenobio A, Rossi S, Chiarelli S, Spadoni M, Wesche R and Bruzzone P L 2003 High performance new MgB₂

- superconducting hollow wires *Supercond. Sci. Technol.* **16** 285.
- [13] Giunchi G 2003 High density MgB₂ obtained by reactive liquid Mg infiltration *Int. J. Mod. Phys. B* **17** 453.
- [14] Saglietti L, Orecchia C, Albisetti A F, Perini E and Giunchi G 2011 Microstructure of the MgB₂ wires resulting by the infiltration process *IEEE Trans. Appl. Supercond.* **21** 2655.
- [15] Shimada Y, Kubota Y, Hata S, Ikeda K, Nakashima H, Matsumoto A, Togano K and Kumakura H 2011 Electron microscopy observations of MgB₂ wire prepared by an internal Mg diffusion method *Physica C* **471** 1137.
- [16] Li G Z, Yang Y, Susner M A, Sumption M D and Collings E W 2012 Critical current densities and *n*-values of MgB₂ strands over a wide range of temperatures and fields *Supercond. Sci. Technol.* **25** 025001.
- [17] Ekin J W 2006 *Experimental techniques for low-temperature measurements: cryostat design, material properties, and superconductor critical-current testing* 1st edn (New York: Oxford University Press)
- [18] Saglietti L, Perini E, Albisetti A F, Ripamonti G, Schiavone C and Giunchi G 2012 MgB₂ doping by rare-earth metals and borides *IEEE Trans. Appl. Supercond.* **22** 6200504.
- [19] Ye S J, Song M, Matsumoto A, Togano K, Zhang Y, Kumakura H, Takeguchi M, Teranishi R and Kiyoshi T 2012 Enhancing the critical current properties of internal Mg diffusion-processed MgB₂ wires by Mg addition *Supercond. Sci. Technol.* **25** 125014.
- [20] Togano K, Hur J, Matsumoto A and Kumakura H 2010 Microstructures and critical currents of single- and multi-filamentary MgB₂ superconducting wires fabricated by an internal Mg diffusion process *Supercond. Sci. Technol.* **23** 085002.
- [21] Kumakura H, Hur J, Togano K, Matsumoto A, Wada H and Kimura K 2011 Superconducting properties of diffusion-processed multifilamentary MgB₂ wires *IEEE Trans. Appl. Supercond.* **21** 2643.
- [22] Giunchi G, Ripamonti G, Perini E, Cavallin T and Bassani E 2007 Advancements in the reactive liquid Mg infiltration technique to produce long superconducting MgB₂ tubular wires *IEEE Trans. Appl. Supercond.* **17** 2761.
- [23] Ye S J, Matsumoto A, Togano K and Kumakura H 2011 Enhancement of the critical current density of internal Mg diffusion processed MgB₂ wires by the addition of both SiC and liquid aromatic hydrocarbon *Physica C* **471** 1133.
- [24] Li G Z, Sumption M D, Susner M A, Yang Y, Reddy K M, Rindfleisch M A, Tomsic M J, Thong C J and Collings E W 2012 The critical current density of

- advanced internal-Mg-diffusion-processed MgB₂ wires *Supercond. Sci. Technol.* **25** 115023.
- [25] Giunchi G 2008 The reactive Mg-liquid infiltration to obtain long superconducting MgB₂ cables *Workshop on Accelerator Magnet Superconductors, Design and Optimization, CERN, Geneva, Switzerland* 83.
- [26] Marzik J V, Suplinskas R J, Wilke R H T, Canfield P C, Finnemore D K, Rindfleisch M, Margolies J, Hannahs S T 2005 Plasma synthesized doped B powders for MgB₂ superconductors *Physica C* **423** 83.
- [27] Susner M A, Yang Y, Sumption M D, Collings E W, Rindfleisch M A, Tomsic M J and Marzik J V 2011 Enhanced critical fields and superconducting properties of pre-doped B powder-type MgB₂ strands *Supercond. Sci. Technol.* **24** 012001.
- [28] Tomsic M, Rindfleisch M, Yue J, McFadden K, Doll D, Phillips J, Sumption M D, Bhatia M, Bohnenstiehl S and Collings E W 2007 Development of magnesium diboride (MgB₂) wires and magnets using *in situ* strand fabrication method *Physica C* **456** 203.
- [29] Dou S X, Pan A V, Zhou S, Ionescu M, Liu H K and Munroe P R 2002 Substitution-induced pinning in MgB₂ superconductor doped with SiC nanoparticles *Supercond. Sci. Technol.* **15** 1587.
- [30] Mikheenko P, Chen S K and MacManus-Driscoll J L 2007 Minute pinning and doping additions for strong, 20 K, in-field critical current improvement in MgB₂ *Appl. Phys. Lett.* **91** 202508.
- [31] Wilke R H T, Bud'ko S L, Canfield P C, Finnemore D K, Suplinskas R J and Hannahs S T 2004 Systematic effects of carbon doping on the superconducting properties of Mg(B_{1-x}C_x)₂ *Phys. Rev. Lett.* **92** 217003.
- [32] Dou S X, Braccini V, Soltanian S, Klie R, Zhu Y, Li S, Wang X L and Larbalestier D 2004 Nanoscale-SiC doping for enhancing J_c and H_{c2} in superconducting MgB₂ *J. Appl. Phys.* **96** 7549.
- [33] Dou S X, Pan A V, Zhou S, Ionescu M, Wang X L, Horvat J, Liu H K and Munroe P R 2003 Superconductivity, critical current density, and flux pinning in MgB_{2-x}(SiC)_{x/2} superconductor after SiC nanoparticle doping *J. Appl. Phys.* **94** 1850.
- [34] Kováč P, Hušek I, Kopera L, Melišek T, Rosová A and Dobročka E 2013 Properties of *in situ* made MgB₂ in Nb or Ti sheath *Supercond. Sci. Technol.* **26** 025007.
- [35] Susner M A, Daniels T W, Sumption M D, Rindfleisch M A, Thong C J and Collings E W 2012 Drawing induced texture and the evolution of superconductive properties with heat treatment time in powder-in-tube *in situ* processed MgB₂ strands *Supercond. Sci. Technol.* **25** 065002.

List of Tables

Table 1. Strand Specifications and Heat Treatment Conditions.

Table 2. MgB₂ Areas and MgB₂ Fill Factors of Multifilamentary AIMI Strands.

Table 1. Strand Specifications and Heat Treatment Conditions ^a

Sample name	Trace No. ^b	Sample type ^c	Filament count	Central filament	C mol% ^d	MgB ₂ (%) ^e	FF	Filament to strand fraction (%) ^f	MgB ₂ (%) in filament ^g	dia., mm	H.T., °C /min
<i>Monofilamentary AIMI Samples</i>											
A1	2893I	short	1	-	3	4.2		33.5	12.5	0.55	675/60
A2	2893II	short	1	-	3	5.1		32.2	15.8	0.55	675/120
A3	2893IV	short	1	-	3	5.2		32.5	16.0	0.55	675/240
A4	2909I	short	1	-	4	3.7		31.8	11.0	0.55	675/60
A5	2909II	short	1	-	4	5.0		32.6	15.3	0.55	675/120
A6	2909IV	short	1	-	4	5.0		32.5	15.4	0.55	675/240
<i>Multifilamentary AIMI Samples</i>											
B1	2885I	barrel	18	Cu-Ni	2	13.2		33.8	39.1	0.83	675/60
B2	2885II	barrel	18	Cu-Ni	2	14.4		33.2	43.4	0.83	675/120
B3	2962I	short	18	Cu-Ni	3	13.1		33.0	39.7	0.83	675/60
B4	2962II	short	18	Cu-Ni	3	13.0		33.6	38.7	0.83	675/120
B5	2967I	short	18	Cu-Ni	4	9.8		33.4	29.3	0.83	675/60
B6	2967II	short	18	Cu-Ni	4	12.0		34.4	34.9	0.83	675/120
<i>Multifilamentary PIT Samples</i>											
P1	2555	barrel	36	Cu	2	25.0		25.0	100	0.92	700/60
P2	2510	barrel	36	Cu	2.5	22.6		22.6	100	0.92	675/60
P3	2580	barrel	36	Cu	3	17.8		17.8	100	0.91	650/120
P4	2538	barrel	36	Cu	3.5	25.8		25.8	100	0.91	675/60
P5	2535	barrel	36	Cu	4	26.9		26.9	100	0.91	675/60

^aAll the strands, fabricated by HTR, incorporated a Nb chemical barrier and Monel outer sheath.

^bSample number for internal purpose.

^cAs explained in Section 2.2, “barrel” means a one-meter-long segment helically wound onto 32-mm-diameter Ti-Al-V holder; “short” means a 50 mm long straight wire.

^dC doping level, which is based on C analysis by the LECO Corporation and normalized to the molar weight of MgB₂. No assumptions are made here concerning the expected uptake of C into the B sublattice; see, [27].

^eNamely the MgB₂ fill factor, which is the transverse cross-sectional area fraction of MgB₂ in the whole strand, based on scanning electron microscopy (SEM) and optical microscopy (OM) images. Hence, MgB₂ FF = MgB₂ layer area / overall wire area. The “layer J_c ” is estimated according to “MgB₂ FF”.

^fThe “Filament to strand fraction” in the non-barrier area fraction in the whole strand, i.e. “Filament to strand fraction” = the cross-sectional area of everything within the Nb chemical barrier area (not including Nb) / overall wire area.

^gThe “MgB₂ (%) in filament” = MgB₂ layer area / the cross-sectional area of everything within the Nb chemical barrier area (not including Nb).

Table 2. MgB₂ Areas and MgB₂ Fill Factors of Multifilamentary AIMI Strands.

Sample name	MgB ₂ area, μm^2	error, μm^2 + / -	MgB ₂ fill factor, %	error, % + / -
B1	71600	2700 / 2200	13.2	0.5 / 0.4
B2	77800	3900 / 1200	14.4	0.7 / 0.2
B3	70800	700 / 1500	13.1	0.1 / 0.3
B4	70500	1300 / 3700	13.0	0.2 / 0.7
B5	52900	3100 / 300	9.8	0.6 / 0.1
B6	65400	2500 / 2500	12.0	0.5 / 0.5

List of Figures

Figure 1 Field dependence of the layer J_c s of the 3 mol% and 4 mol% C doped monofilamentary AIMI strands at 4.2 K. Also included is a previously reported 2 mol% C doped “2G-IMD” strand HTed at 675 °C for 1 hour [24].

Figure 2 (a) Optical microscopic and (b) back scattered SEM images taken from the same transverse cross section in the 3 mol% C doped AIMI strand A3.

Figure 3 Field dependence of the non-barrier J_c s of the 3 mol% and 4 mol% C doped monofilamentary AIMI strands at 4.2 K. A fully transformed 2 mol% C doped “2G-IMD” strand is included [24].

Figure 4 Transverse cross-sectional (a) SEM and (b) OM images of the 2 mol% C doped multifilamentary AIMI strand B1.

Figure 5 Field dependence of the layer J_c s for multifilamentary AIMI strands at 4.2 K, data from P3 and P4 are included for comparison. Here B1 and B2 are one-meter-long “ITER-barrel” type strands.

Figure 6 Field dependence of the non-barrier J_c s for multifilamentary AIMI strands at 4.2 K, data from P3 and P4 are included for comparison. Here B1 and B2 are one-meter-long “ITER-barrel” type strands.

Figure 7 Field dependence of the engineering J_e s for multifilamentary AIMI strands at 4.2 K, data from P3 and P4 are included for comparison. Here B1 and B2 are one-meter-long “ITER-barrel” type strands.

Figure 8 Comparison and relationships between J_e , layer J_c and MgB₂ fill factor (FF) of multifilamentary AIMI strands and PIT strands with different C concentrations at 4.2 K, 10 T. Error bars are added for AIMI strands to describe the accuracy of the data.

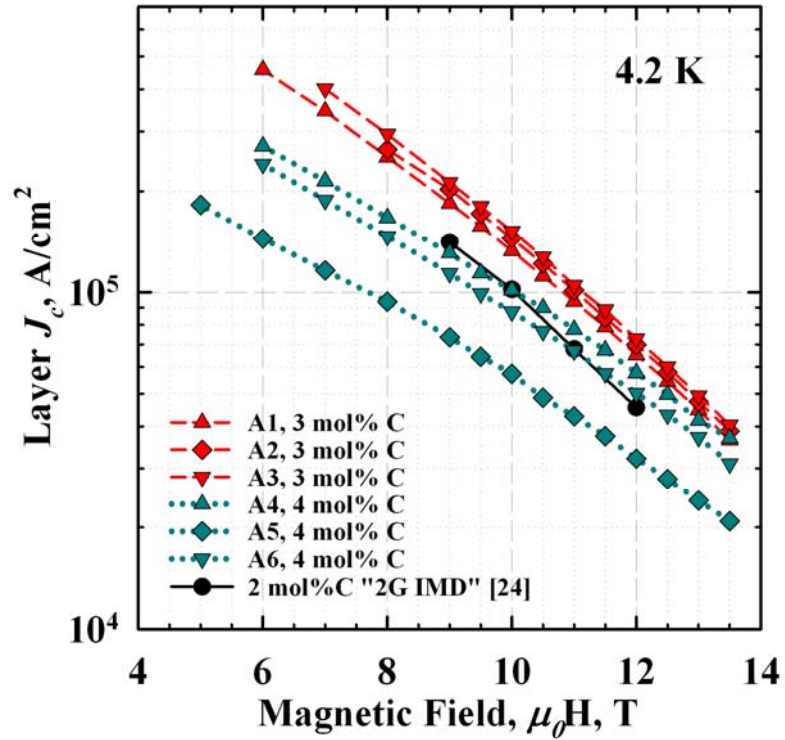


Figure. 1 Field dependence of the layer J_c s of the 3 mol% and 4 mol% C doped monofilamentary AIMI strands at 4.2 K. Also included is a previously reported 2 mol% C doped “2G-IMD” strand HTed at 675 °C for 1 hour [24].

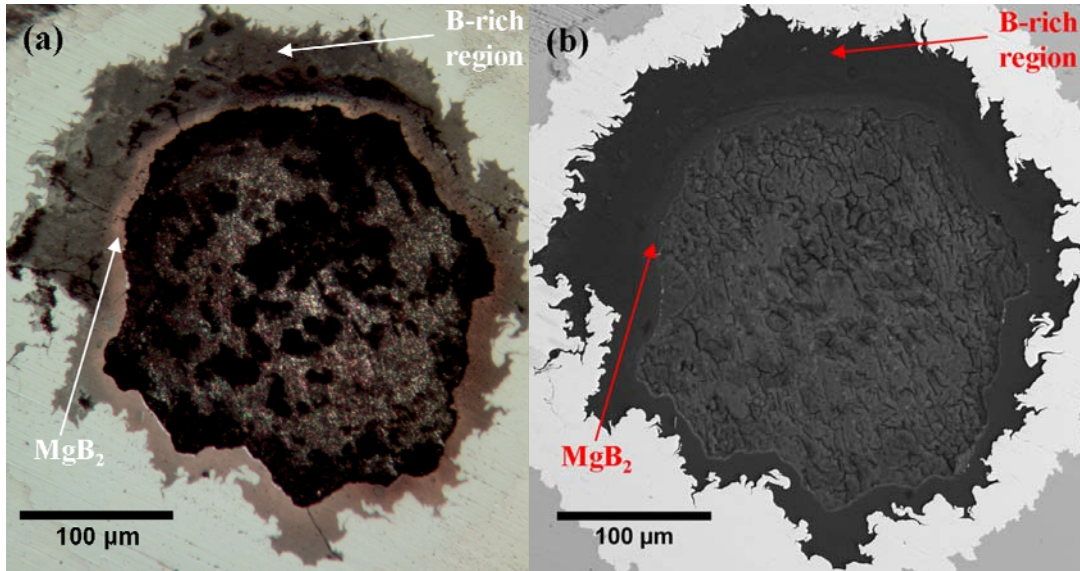


Figure. 2 (a) Optical microscopic and (b) back scattered SEM images taken from the same transverse cross section in the 3 mol% C doped AIMI strand A3.

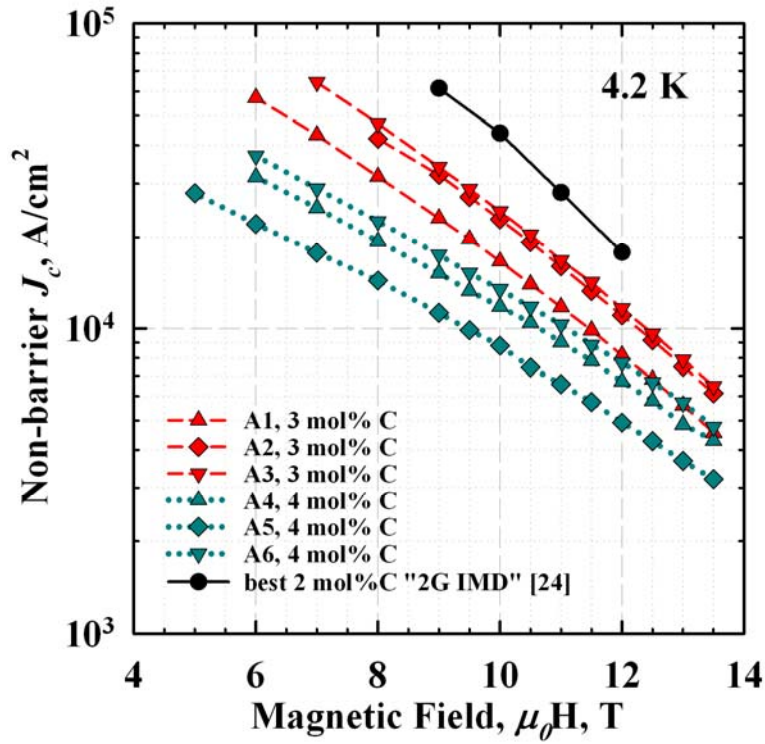


Figure. 3 Field dependence of the non-barrier J_c s of the 3 mol% and 4 mol% C doped monofilamentary AIMI strands at 4.2 K. A fully transformed 2 mol% C doped “2G-IMD” strand is included [24].

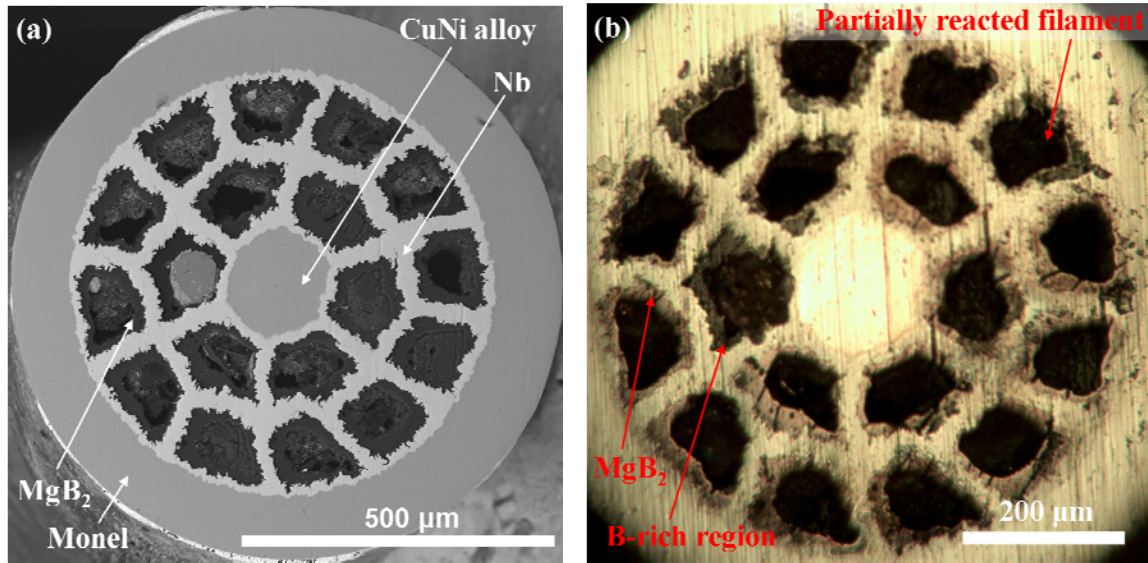


Figure. 4 Transverse cross-sectional (a) SEM and (b) OM images of the 2 mol% C doped multifilamentary AIMI strand B1.

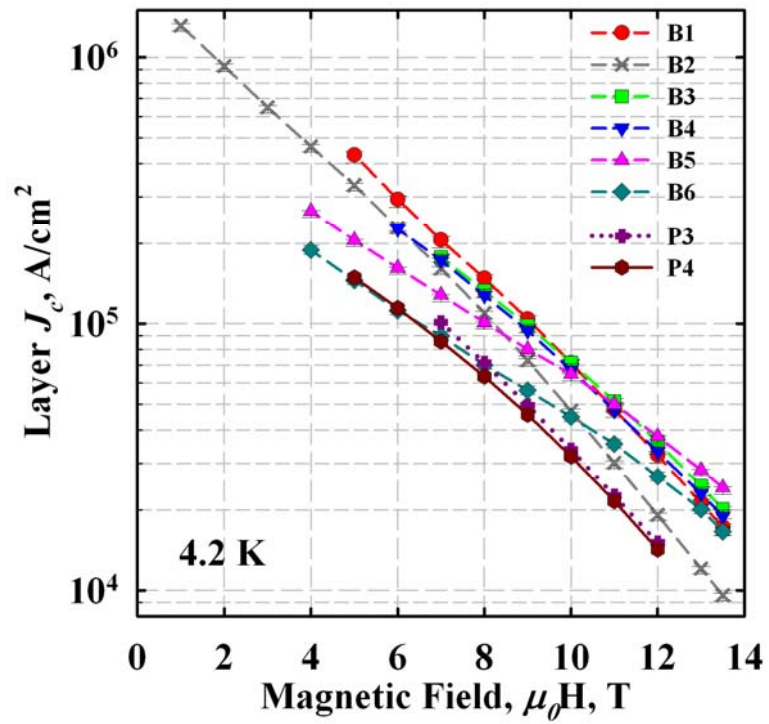


Figure 5. Field dependence of the layer J_c s for multifilamentary AIMI strands at 4.2 K, data from P3 and P4 are included for comparison. Here B1 and B2 are one-meter-long “TER-barrel” type strands.

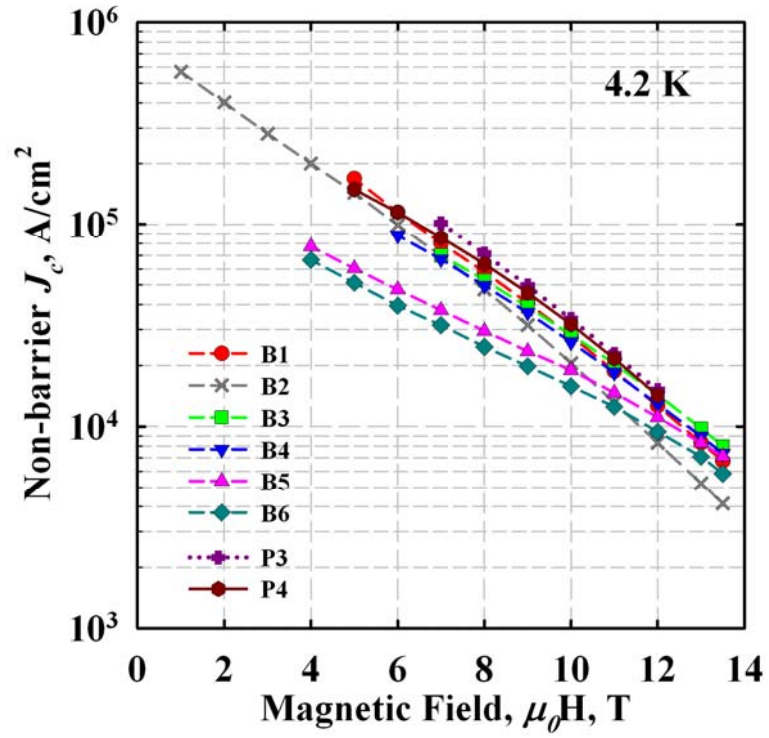


Figure 6. Field dependence of the non-barrier J_c s for multifilamentary AIMI strands at 4.2 K, data from P3 and P4 are included for comparison. Here B1 and B2 are one-meter-long “ITER-barrel” type strands.

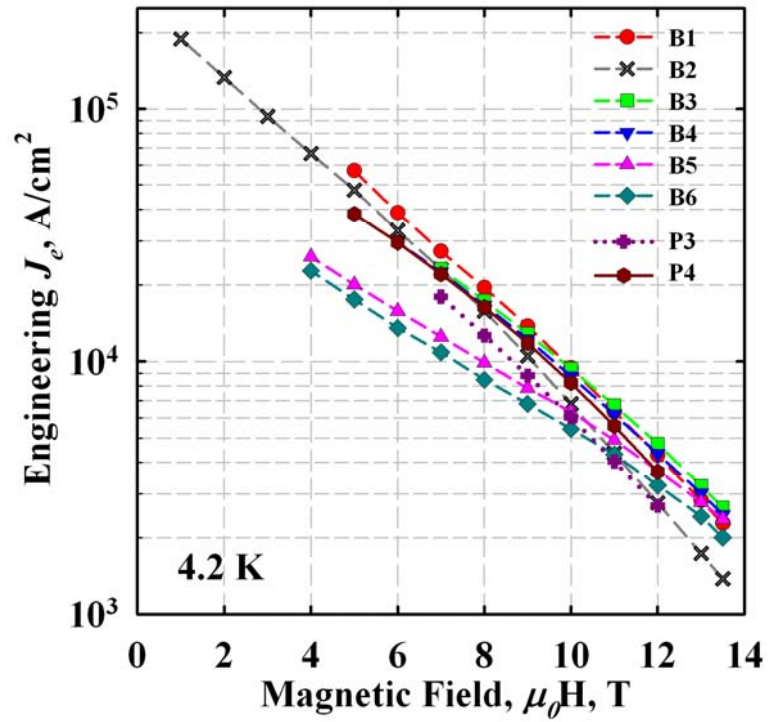


Figure 7. Field dependence of the engineering J_e s for multifilamentary AIMI strands at 4.2 K, data from P3 and P4 are included for comparison. Here B1 and B2 are one-meter-long “ITER-barrel” type strands.

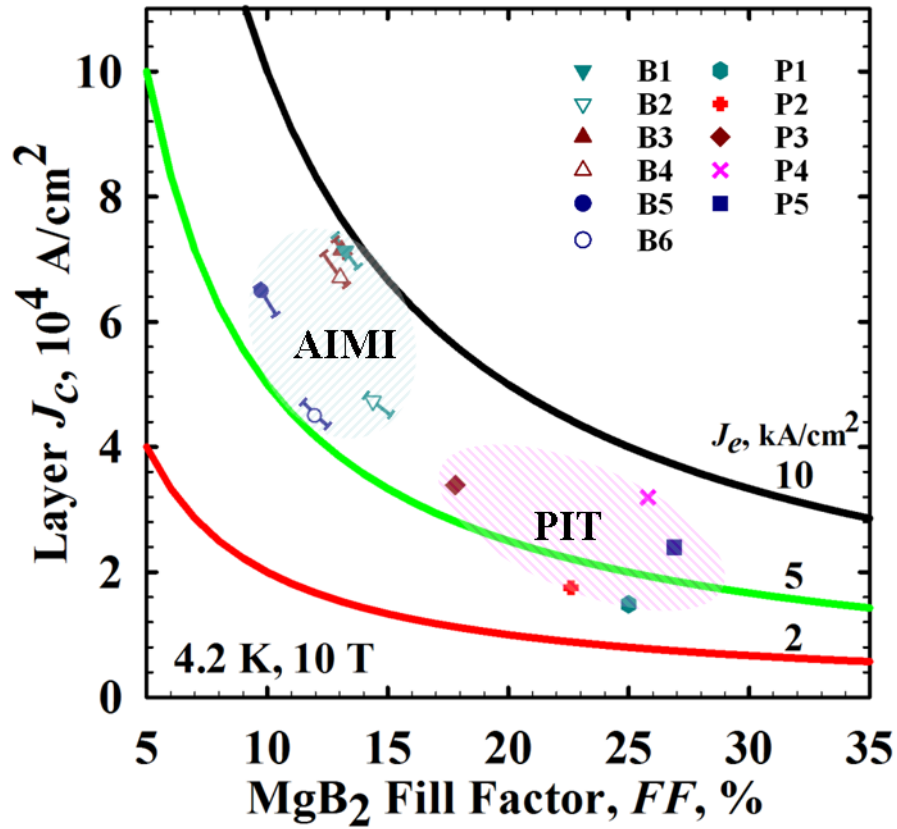


Figure 8. Comparison and relationships between J_e , layer J_c and MgB_2 fill factor (FF) of multifilamentary AIMI strands and PIT strands with different C concentrations at 4.2 K, 10 T. Error bars are added for AIMI strands to describe the accuracy of the data.